IEEE Access
Multidisciplinary | Rapid Review | Open Access Journal

Received February 11, 2021, accepted March 7, 2021, date of publication March 10, 2021, date of current version March 19, 2021.

Digital Object Identifier 10.1109/ACCESS.2021.3065265

Design and Performance Investigation of 3-Slot/2-Pole High Speed Permanent Magnet Machine

HAMID ALI KHAN[1], FAISAL KHAN[1], (Member, IEEE), SURAT KHAN[2], NASEER AHMAD[2], JAHANGEER BADAR SOOMRO[3], AND IRFAN SAMI[4]

[1]Department of Electrical and Computer Engineering, COMSATS University Islamabad–Abbottabad, Abbottabad 22060, Pakistan
[2]Faculty of Information and Communication Technology, Balochistan University of Information Technology, Engineering and Management Sciences (BUITEMS), Quetta 87300, Pakistan
[3]Department of Electrical Engineering, Sukkur IBA University, Sukkur 65200, Pakistan
[4]School of Electrical and Electronics Engineering, Chung-Ang University, Seoul 06974, South Korea

Corresponding author: Hamid Ali Khan (hamidalims@gmail.com)

This work was supported by the COMSATS University Islamabad–Abbottabad, and in part by the Higher Education Commission of Pakistan under Grant TDF 03-067/R&D/HEC/ 2019.

ABSTRACT High-speed rotating mechanical machinery is a developed, mature and reliable technology for many engineering applications. In high-speed permanent magnet machines, the rotor's permanent magnet PM is not strong enough to withstand the centrifugal force resulting from excessive rotational speed; thus, the PM material must be protected by a non-magnetic alloy sleeve. This paper presents a novel high-speed PM machine with solid rotor PM covered by a titanium retaining sleeve. The rotor stress condition is simplified as a plane stress problem according to the strength measurement of solid PM rotors in the high-speed PM motors. The analytical formulas for rotor stress are presented based on the polar coordinate displacement method. The proposed model is compared with a conventional model having auxiliary slots in stator teeth. Using a finite element analysis environment, the performance analysis shows that the proposed design has reduced magnet eddy current loss, cogging torque, and iron losses. The initial design is also optimized using a deterministic optimization algorithm that increases output torque by 26% compared to the initial design.

INDEX TERMS Airgap flux density, finite element method, high-speed permanent magnet machine, magnet eddy current loss, retaining sleeve, rotor design, stress analysis.

I. INTRODUCTION

The electrical machines operating at high speed have been made possible with advancements in power electronic converters. The benefit of such development is that it is possible to reduce the machine's size with a given power rating. Such machines are used in various areas, including compressors, air blowers, aircraft, and automotive applications. The idea of high-speed electrical machines is further strengthened by advanced production techniques and accessibility of high specification materials. However, such advantages are not for free as the machine mechanical limitation and overheating become a significant problem for the machine designer. Therefore, several iterations must be accomplished before compromise converges between the disciplines mentioned above [1], [2].

In the last decades, the research communities highly interested in high-speed PM machines. PM machines have become very popular in real-time applications with the research advancement of rare-earth magnet materials. Based on the particular requirement of applications and specifications, 2 or 4 poles are recommended for a high-speed rotor. In low power ultra-high-speed operations, the 2-pole rotor configuration is selected owing to the lesser fundamental frequency. The 2-pole rotor design can easily control and reduce iron and magnet eddy current loss [3], [4]. However, several challenges occur in the manufacturing of high-speed PM machines due to the replacement of field winding by PM. In advanced high-speed PM machines, a parasitic loss is considered rotor eddy loss, as it only contributes to a small amount of the machine's overall power [5], [6]. Precise calculation

The associate editor coordinating the review of this manuscript and approving it for publication was Sanjeevikumar Padmanaban.

of eddy current loss is essential in PM machines for high performance and efficiency. Asynchronous harmonics causes eddy current loss in PM machine; such harmonics are time and spatial harmonics. Therefore, it is vital to eliminate the time and spatial harmonics of the PM machine [7], [8].

Various machine designs were proposed to suppress rotor eddy current loss. By enlarging the airgap length, these losses were reduced [9], [10]; but it affects the machine power density. Eddy current paths can be break by using segmentation and skewing techniques, which eliminates rotor eddy current losses; however, due to the complex structure, the fabrication of these machines is difficult and costly [11], [12].

Various techniques are applied for estimating and minimizing eddy current losses, such as the different configurations of winding, rotor structure optimization, a shield of copper, and covering PM by conductive enclosure [13]–[15]; however, rotor total losses are increasing with these methods. Another way to suppress the airgap permeance harmonics that caused losses is to use the PWM technique [16]; however, only time harmonics reduces in this case. Auxiliary slots in the stator teeth are proposed by [17] to reduce the PM eddy current loss, which partially decreases PM losses without lowering the amplitude of the spatial harmonics.

Specific designs were suggested in [18] and [19], which substitute the machine's shaft with a solid permanent magnet. A protecting enclosure is used to shield the PM and connect the shafts from both sides, as illustrated in Fig. 1. A highly strengthened and resistive materials enclosure, such as carbon fiber composite (CFC), stainless steel, and titanium, can reduce the eddy current loss with PM safety provision [20]. Moreover, for the rated working condition, the enclosure width can be kept minimum so that the amplitude of airgap flux density affect slightly. To stabilize the stress, the width of protecting enclosure and rotor stress must be correctly calculated; otherwise, the rotor damages significantly.

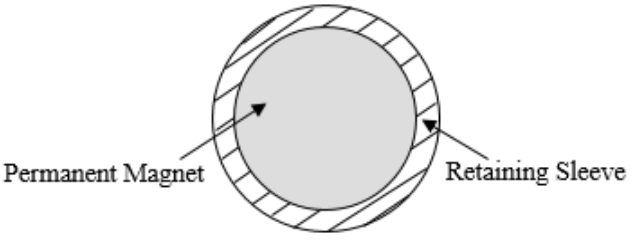

FIGURE 1. Proposed rotor topology.

The conductivity of the enclosure mainly influences the distribution of rotor eddy current losses. With the enclosure's high conductivity, PM eddy current loss is minimized highly. Utilizing the benefit of this method, a highly conductive enclosure has used; however, it increases rotor temperature and total losses [21].

The rotor parts can experience considerable centrifugal force and a certain amount of thermal stress at high-speed operating conditions. Therefore, the primary issue for high-speed PM machines in terms of mechanical reliability is stress analysis. Stress computation techniques are categorized into finite element and analytical analysis. Reference [22], [23] use the finite element method, while numerous other research articles proposed an analytical computation model [24]–[29]. Reference [24] suggested a simplified analytical approach based on the premise that the rotor is severely rotational symmetry. The displacement technique was proposed for the computation of a high-speed PM machine with a non-magnetic alloy enclosure [25] and [26]. The PM rotors are usually modeled as the multifaceted cylinders in most analytical techniques. However, all the above-mentioned analytical methods are valid for short stack length machines due to planer stress utilization.

In achieving stress of each component stress in the rotor, the objective is to assure that specific stress values are in the material temperature and speed range throughout the operating conditions. Therefore, for allowable temperature and speed, the worst operating conditions must be determined for each part of the rotor. Hence, instead of the entire operating range, the rotor stress is calculated only in the rated working condition. The effect of temperature and operating speed on the tangential and radial stress of enclosure and PM has been thoroughly examined in [30], [31] stated that the thermal expansion must be addressed due to the considerable effect in the enclosure tangential stress.

This paper proposed a 3-slot/2-pole high-speed PM machine model using a titanium enclosure over the solid PM rotor to reduce magnet eddy current loss, cogging, and iron losses and investigate the rotor sleeve stress. The results are computed by finite element analysis (FEA) and analytical equations for the proposed design and then optimized the proposed model for high output electromagnetic torque at different working conditions.

II. DESIGN METHODOLOGY

The design methodology of the proposed 3-slot/2-pole high-speed permanent magnet machine is investigated using JMAG-Designer as a 2D FEA solver to evaluate the electromagnetic performance of the motor. A 2-pole rotor design is selected to confine the fundamental frequency. A solid PM rotor is used instead of a surface-mounted PM for dynamic balance and easy manufacturing. Throughout their operation, the losses present in these machines are of great concern. The behavior and magnetic properties of the materials used in the manufacturing of the rotor and stator of such machines must be considered in the design process of these machines.

Initially, the design process and setting conditions of the proposed topology are elaborated. The methodology and several specific conditions in investigating the proposed design's performance at different working conditions are also carried out. The armature current density of the proposed model is calculated as:

$$J_a = \frac{N_a I}{S\alpha} \tag{1}$$

where J_a, N_a, I, S, and α are current density, number of turns, RMS current, area of the slot, and filling factor, respectively.

TABLE 1. Design parameters.

Geometry Parameter	Value	Geometry Parameter	Value
Rated-current	10 A	Outer diameter of the stator	50 mm
Width of AS	0.549 mm	Outer diameter of the rotor	17 mm
Depth of AS	9.540 mm	Opening of slot	2 mm
Stator Core	Silicon Steel (35H210)	Sleeve Material	Titanium
Axial length	30 mm	Diameter of PM	14.1 mm
Magnetic material	NEOMAX-35AH	Number of Poles	2
Rated speed	60000 rpm	Length of airgap	0.6 mm
Number of turns	32 turns	Height of yoke	5.2 mm

From Eq. 1, it shows that the number of turns directly depends upon the slot area. For winding configuration, the concentrated non-overlap winding design is selected, decreasing copper losses and improving the proposed model's efficiency.

The proposed design shaft is shortened by PM, taking the magnet volume equal to the conventional model, and a titanium enclosure is used over it to bound the PM between the shaft. The titanium enclosure width in the proposed design is considered according to the outer diameter of the existing design. Various materials, such as carbon fiber composite (CFC), titanium, and copper, can also be used for the enclosure. Owing to the low flexibility stiffness of CFC; consequently, due to the reliance on bending stability, crucial speed, and relatively low thermal conductivity, it is not preferred for the enclosure. Highly rigid titanium material is selected for the enclosure to reduce the PM losses pertaining to the proposed motor's rigidity and high speed.

In contrast with CFC, titanium metallic enclosure is fitted with a comparatively lower strength to density ratio. The titanium material enclosure also benefits from lower cost and higher electrical and thermal conductivity; therefore, the eddy current loss will present in titanium sleeves instead of PM. In addition to the thermal and electromagnetic aspects, such as mitigation of rotor losses, the enclosure option should also consider the mechanical factors, including magnet protection and penetration of harmonics into the PM, it acts as a shield.

There are some restrictions and specifications to be followed in order to design a motor. The summary of overall restrictions and specifications is as shown in Table. 1, and Table. 2. The structural view of conventional and proposed designs is shown in Fig. 2 (a) and (b).

In this design, the target performance to reduced cogging torque and magnet eddy current loss is expected to achieve, using the exact specification with the conventional design. The rated armature current density, $J_{a,}$ is set to 4.47A/mm^2. Therefore, the proposed design obtained reduced magnet eddy current loss, iron loss and cogging torque, and enhance output torque at various operating conditions.

The performances of the initial design that have been successfully developed are then evaluated and analyzed.

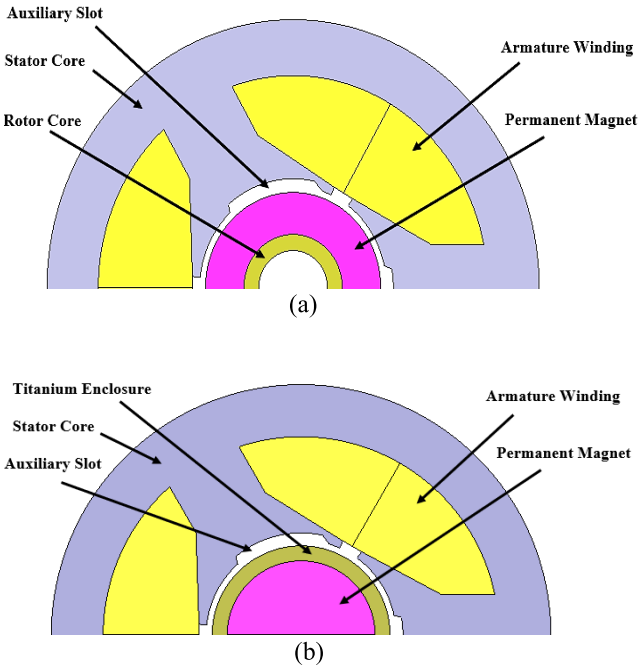

FIGURE 2. 2D view of (a) conventional design, and (b) proposed model.

TABLE 2. Sleeve material properties.

Properties	Value
Material	Titanium
Young's Modulus (GPa)	110
CTE (1/K)	8.45E-6
Thermal Conductivity (W/(m . k))	7.5
Poisson's Ratio	0.31
Allowable Stress (MPa)	480
Density (kg/m^3)	4400
Conductivity (S/m)	5.6E+5

The investigation is divided into two parts, which are no-load and load analysis. Under the no-load study, cogging torque characteristics, flux linkage characteristics, flux distribution, flux lines, and eddy current loss in PM are investigated. At different armature, current density conditions, the maximum output torque, iron loss, and eddy current loss in PM are examined for load analysis. Fig. 3 illustrates the implementation procedure of the proposed design for FEA analysis.

III. PROPOSED STRESS ANALYSIS OF RETAINING SLEEVE

For sleeve stress analysis, we use the model presented in [32]. As a plane stress problem, we simplify the rotor stress condition. The analytical formulas of rotor stress are obtained by solving the differential equation of stress for the non-magnetic alloy enclosure.

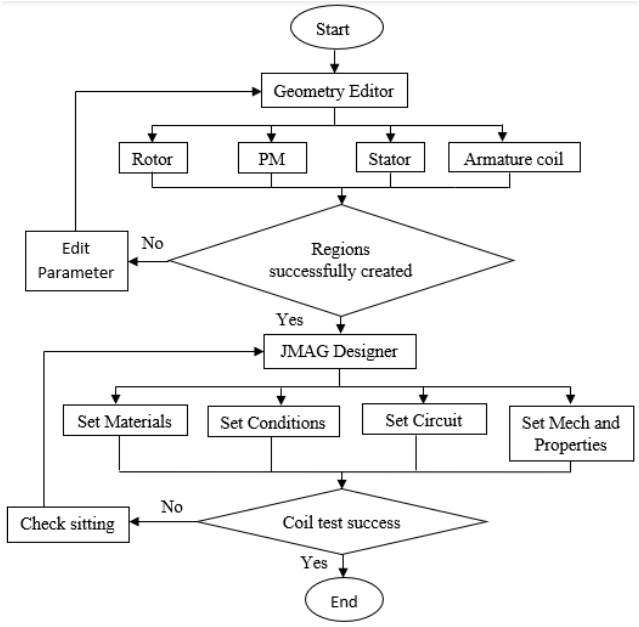

FIGURE 3. Design procedure.

Using elastic mechanics theory, equilibrium differential equation of non-magnetic alloy sleeve is

$$\frac{d\sigma_{rh}}{dr} + \frac{\sigma_{rh} - \sigma_{\theta h}}{r} + \sigma_h \omega^2 r = 0 \tag{2}$$

where,

$\sigma_{\theta h}$ and σ_{rh} are the tangential and radial stress of enclosure in the radius of r, respectively.

ρ_h; is density,

ω; velocity$_{(\text{angular})}$,

After considering the temperature rise of sleeve material, one gets the following relation:

$$\begin{cases} \varepsilon_{rh} = \dfrac{1}{E_h}\left(\sigma_{rh} - \mu_h \sigma_{\theta h}\right) + \beta_h . \Delta T_h \\ \varepsilon_{\theta h} = \dfrac{1}{E_h}\left(\sigma_{\theta h} - \mu_h \sigma_{rh}\right) + \beta_h . \Delta T_h \end{cases} \tag{3}$$

where,

ε_{rh}; radial strain,

ε_{rh}; tangential strain,

E_h; Young's modulus,

μ_h; Poisson's ratio,

β_h; thermal expansion coefficient,

$\Delta T_h = T_h(r) - T_{h0}(r)$,

$T_h(r)$; temperature of sleeve at high speed,

$T_{h0}(r)$; temperature of sleeve at an initial time,

The geometric equation of sleeve material is

$$\begin{cases} \varepsilon_{rh} = \dfrac{du_h}{dr} \\ \varepsilon_{\theta h} = \dfrac{u_h}{r} \end{cases} \tag{4}$$

where,

μ_h; radial displacement of the sleeve in radius r,

Combining eq. (3) with (4) yields:

$$\begin{cases} \sigma_{rh} = \dfrac{E_h}{1-\mu_h^2}\left[\dfrac{du_h}{dr} + \mu_h \dfrac{u_h}{r} - (1+\mu_h)\,\beta_r \cdot \Delta T_h\right] \\ \sigma_{\theta h} = \dfrac{E_h}{1-\mu_h^2}\left[\dfrac{u_h}{r} + \mu_h \dfrac{du_h}{dr} - (1+\mu_h)\,\beta_h \cdot \Delta T_h\right] \end{cases} \tag{5}$$

From eq. (2) and (5) we obtain:

$$\frac{d^2 u_h}{du^2} + \frac{1}{r}\frac{du_h}{dr} - \frac{u_h}{r^2} = \beta_h (1+\mu_h)\frac{d(\Delta T_h)}{dr} - \frac{\rho_h \omega^2 r\left(1-\mu_h^2\right)}{E_h} \tag{6}$$

By solving Eq. (6), we can obtain:

$$u_h(r) = C_{1h} r + \frac{C_{2h}}{r} - \frac{\rho_h \omega^2 r^3\left(1-\mu_h^2\right)}{8E_h} + \beta_h (1+\mu_h)\frac{1}{r}\int_{Rhi}^{r} \Delta T_h \cdot r dr \tag{7}$$

where the coefficient C_{1h} and C_{2h} are undetermined.

Putting eq. (7) in (5), we can achieve the tangential and radial stresses of the sleeve:

$$\sigma_{rh}(r) = -\frac{E_h \beta_h}{r^2}\int_{R_{hi}}^{r} \Delta T_h \cdot r dr + \frac{E_h}{1-\mu_h^2}\left[C_{1h}(1+\mu_h) + C_{2h}(\mu_h - 1)\frac{1}{r^2}\right] - \frac{\rho_h \omega^2 r^2 (3+\mu_h)}{8} \tag{8}$$

$$\sigma_{\theta h}(r) = \frac{E_h \beta_h}{r^2}\int_{R_{hi}}^{2} \Delta T_h \cdot r dr - \beta_h \cdot \Delta T \cdot E_h + \frac{E_h}{1-\mu_h^2}\left[C_{1h}(1+\mu_h) + C_{2h}(1-\mu_h)\frac{1}{r^2}\right] - \frac{\rho_h \omega^2 r^2 (3\mu_h + 1)}{8} \tag{9}$$

From Eq. (8) and (9), we can compute Von-Mises stress of the non-magnetic alloy sleeve:

$$\sigma_{hMises} = \sqrt{\frac{1}{2}\left[(\sigma_{rh} - \sigma_{\theta h})^2 + (\sigma_{rh})^2 + (\sigma_{\theta h})^2\right]} \tag{10}$$

The boundary condition of the stress of the sleeve is

$$\begin{cases} \sigma_{rh}|_{r=R_{hi}} = -P \\ \sigma_{rh}|_{r=R_{h0}} = 0 \end{cases} \tag{11}$$

Substituting Eq. (8) into (11), we get the undetermined coefficients C_{1h} and C_{2h}:

$$C_{1h} = \frac{-P \cdot (1-\mu_h)}{E_h\left(1-\alpha_h^{-2}\right)} - \frac{(1-\mu_h)\beta_h}{R_{hi}^2\left(1-\alpha_h^{-2}\right)}\int_{R_{hi}}^{R_{h0}} \Delta T_h \cdot r dr + \frac{\rho_h \omega^2 R_{h0}^2 (3-\mu_h)\left(\alpha_h^2 + 1\right)}{8E_h} \tag{12}$$

where $\alpha_h = \frac{R_{hi}}{R_{h0}}$;

$$C_{2h} = \frac{-P \cdot (1+\mu_h) R_{hi}^2}{E_h \left(\alpha_h^2 - 1\right)} - \frac{(1+\mu_h)\, \beta_h R_{hi}^2}{R_{h0}^2 \left(\alpha_h^2 - 1\right)} \int_{R_{hi}}^{R_{h0}} \Delta T_h \cdot rdr + \frac{\rho_h \omega^2 R_{h0}^2 (1+\mu_h)(3+\mu_h) R_{hi}^2}{8E_h} \quad (13)$$

IV. PERFORMANCE ANALYSIS OF PROPOSED DESIGN

The performance analysis of the proposed design is carried out in this section. The workflow of performance investigation is shown in Fig. 4. Initially, the operating principle of novel design is needed to investigate at no-load. The no-load analysis provides excitation only from the permanent magnet and set armature coil current at zero, called coil test analysis. A coil arrangement test analysis is performed to examine each armature coil of the proposed model. Two coils must have identical characteristics during performing a three-phase armature coil arrangement. All coils' directions are arranged so that a sinusoidal waveform is achieved with 120 phase shifted. The generated fluxes are then monitored through each armature coil, and their flux profile is compared with each other.

The FEA analysis performed at the open circuit, contains the investigation of flux linkage, cogging torque, and PM eddy current loss distribution. In contrast, the short circuit analysis includes average PM eddy current loss and electromagnetic torque at various working conditions.

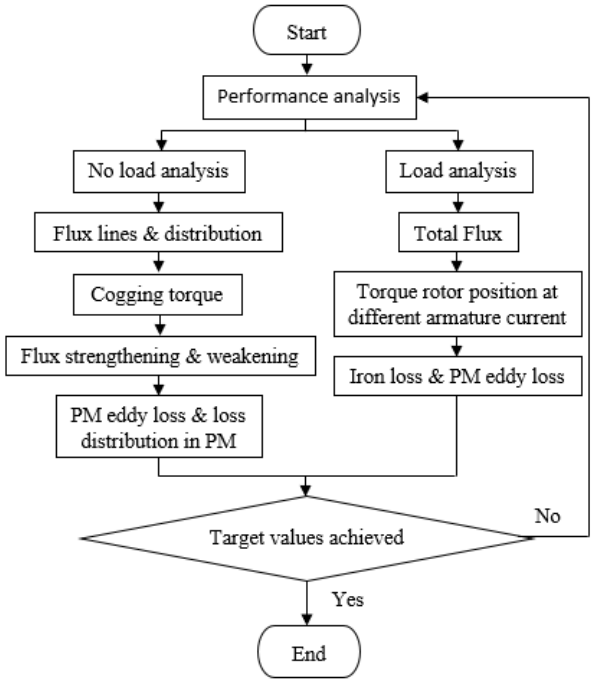

FIGURE 4. Performance analysis procedure.

A. FLUX LINKAGE

Initially, the operating principle of the 3-Slot/2-Pole machine must be validated and investigate the armature coil three-phase system. Fig. 5 shows the peak magnetic flux amplitude of the proposed model obtained is about 10mWb with an almost sinusoidal waveform.

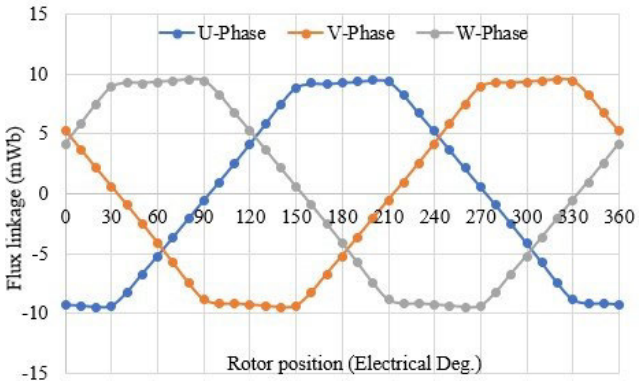

FIGURE 5. Three-phase flux linkage of the proposed design.

In comparison with the existing design, Fig. 6 shows the U-phase flux linkage of the conventional and proposed model. Owing to the addition of enclosure in the proposed design, the flux-linkage of the proposed model is marginal, i.e., 7.4% decreased from the existing design.

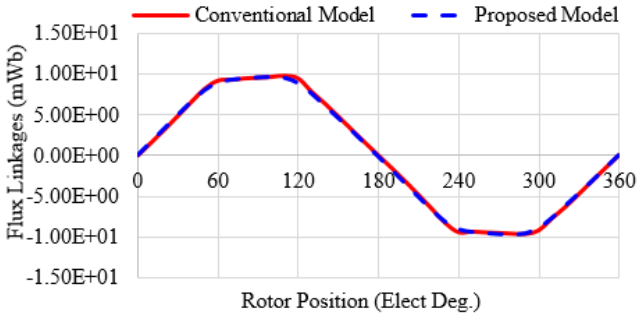

FIGURE 6. Flux linkage of conventional vs. proposed design.

B. EDDY CURRENT LOSS PM

Compared to other machines, PM machines have high core losses. Due to the ferrite magnet's high resistivity, PM eddy current loss is usually neglected in PM machines. In contrast, the rare-earth magnet Nd-Fe-B has a poorer resistivity, which can be demagnetized in high-speed PM machines as the rotor temperature increases. Therefore, a practical calculation of core losses is essential for high efficiency and better performance of PM machines. The 2D FEA analysis of eddy current loss distribution in PM of existing and the proposed model is illustrated in Fig. 7 (a) and (b), respectively. Comparing both models indicates that the distribution of losses is significantly reduced in the proposed design.

The estimated eddy loss of PM is computed by the analytical equations presented in [19] given as follows:

$$P_m \approx \frac{V_m b_m^2 \hat{B}_m^2 \omega^2}{12 \rho_m} \quad (14)$$

where: ω: frequency, ρ_m: resistivity of PM, b_m: PM width, B_m: airgap flux density, V_m: PM volume

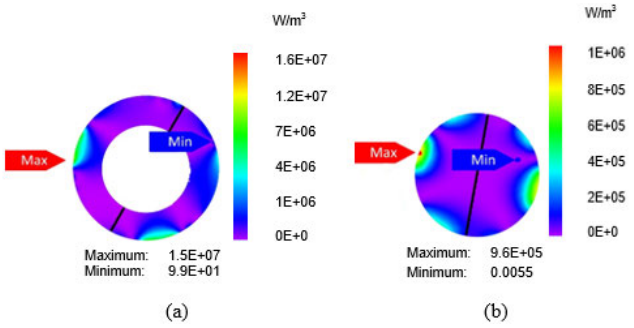

FIGURE 7. 2D distribution of loss in solid PM.

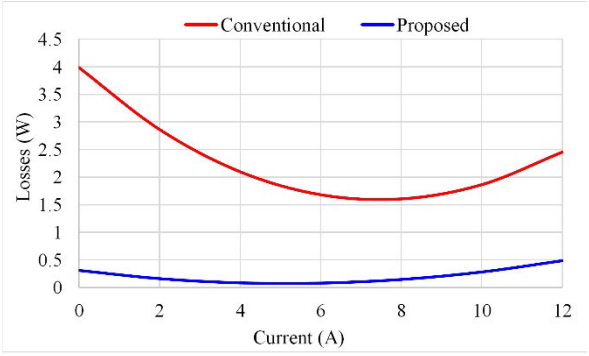

FIGURE 8. PM eddy current loss comparison.

Fig. 8 demonstrates that the magnet eddy current loss of the proposed design is significantly less than the existing design at various input currents. In the existing design, the PM eddy current loss first decreased with rising the amplitude of input current; however, after 10 A of current, the losses increase. These losses follow the same behavior in the proposed design, but the amplitude of magnet eddy current losses were 86.7% decreased than the existing design.

C. COGGING TORQUE

Cogging torque for the proposed machine model at 60000 rpm speed and 0 A/mm^2 armature density J_a is investigated and shown in Fig. 9. It is vital that for better operation and output performance, a motor should have low cogging torque. Fig. 9 shows that the proposed design's cogging torque is 70% lesser than that of the conventional model, which validates the effectiveness of the proposed model.

D. ROTOR STRESS WITH TITANIUM SLEEVE

To attain the precise value of sleeve stress in the proposed 3-Slot/2-Pole high-speed PM machine at 60000 rpm, the 2D FEA analysis of rotor stress is performed. Fig. 10 shows the 2D FE model of stress distribution in titanium sleeve. It can be examined that due to the pre-stress caused by the interference fit, the maximum stress occurs at the contact surface between the sleeve and magnet. The maximum stress of 0.7287 MPa is predicted in the sleeve, much lower than the allowable stress.

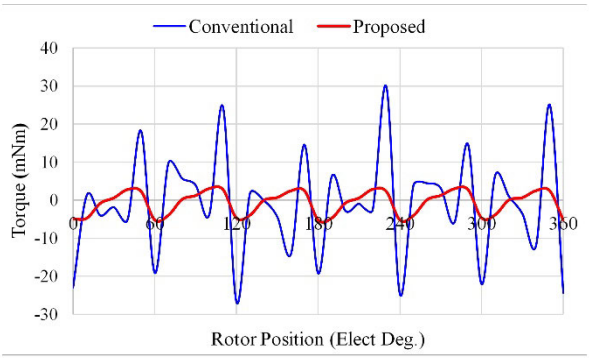

FIGURE 9. Comparison of cogging toque.

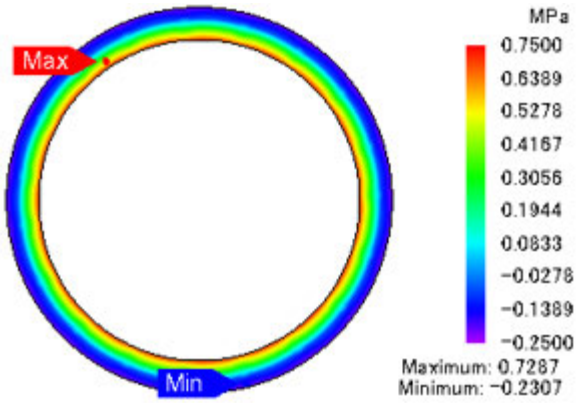

FIGURE 10. Sleeve stress at 60000 rpm.

Hence, for the stress analysis, the proposed 2D FE model is very effective due to less computation time.

E. INSTANTANEOUS TORQUE

Initially, the proposed machine's electromagnetic torque at various rotor positions is examined at optimal J_a condition of 4.405A/mm^2. Instantaneous torque characteristic is achieved when a maximum load was applied. Fig. 11 shows the output electromagnetic torque of the proposed model and reveals that the rated torque has a low torque ripple; however, the torque amplitude is decreased compared to the existing design. The proposed model's output torque is reduced by 20.4% from the conventional design. The average torque reduction is mainly due to the width of the sleeve that reduces the flux linkage strength.

F. IRON LOSSES

Iron losses consist of dynamic and hysteresis losses, such as;

$$\mathcal{P}F_e = \mathcal{P}_d + \mathcal{P}_h \tag{15}$$

where $\mathcal{P}_d$ and $\mathcal{P}_h$ are the dynamics and hysteresis losses, respectively.

According to Eq. (16), the iron losses are depending upon the frequency and magnetic flux density [33],

$$\mathcal{P}_{Fe} = K_h(f, B_m) f B_m^2 + K_e(f, B_m) f^2 B_m^2 \tag{16}$$

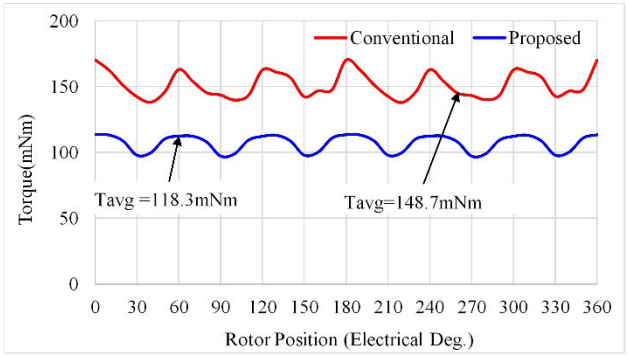

FIGURE 11. Instantaneous torque comparison.

where f, K_e, K_h and B_m are the frequency, coefficient of eddy current losses, coefficient of hysteresis losses, and magnetic flux density, respectively.

The varying flux density in the stator and rotor core that results in iron losses significantly influences the machine electromagnetic performance and output power. The proposed design reduces the variation in the magnetic flux density due to rotor core consumption. The high armature reaction produced by the significantly elevated electric loading increases the motor iron losses. The comparison of iron losses of the conventional and proposed design is shown in Fig. 12, which illustrates that due to consumption of rotor core in the proposed design, the iron losses decrease from 230 W to 127.7 W.

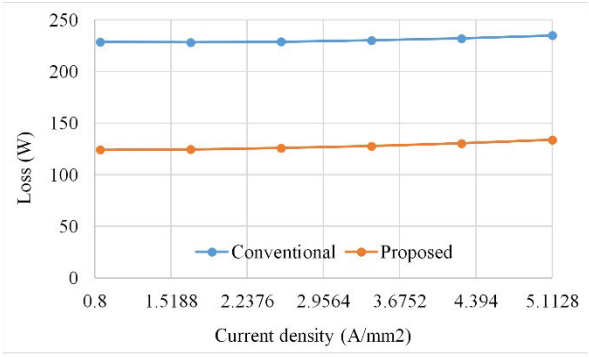

FIGURE 12. Iron loss comparison of the proposed and conventional model.

The time and spatial harmonics are the sources of magnet eddy current loss. The Airgap magnetic field analysis determines spatial harmonics source in the proposed 3-Slot/2-Pole design. The tangential and radial components of airgap flux density distribution at 60000 rpm are shown in Fig. 13 and 14, respectively. The FEA analysis shows that the proposed design eliminates the spatial harmonics considerably compared with the conventional design.

The 2nd spatial harmonic has a high influence on the eddy current loss of PM. The harmonics of airgap flux density were simulated at various operating conditions to investigate the spatial harmonics in detail. It is worth mentioning that the

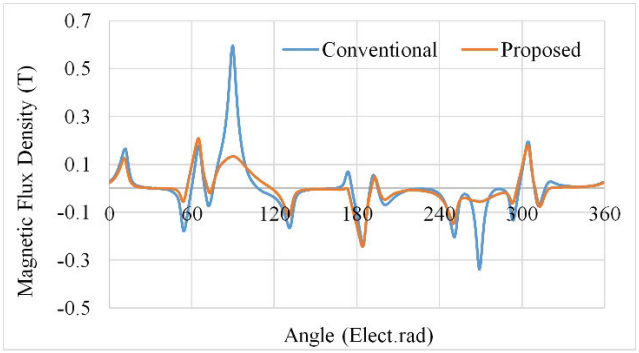

FIGURE 13. Tangential airgap flux density comparison.

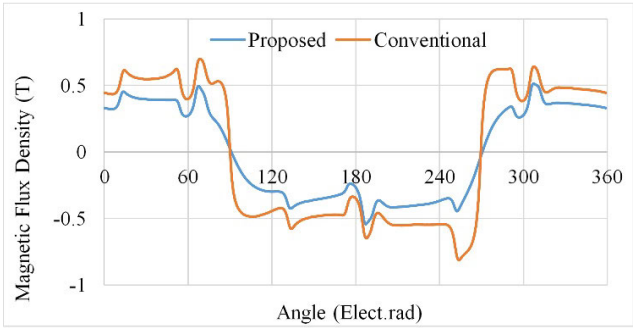

FIGURE 14. Radial airgap flux density of conventional and proposed.

other harmonics have a minor effect on the losses. Therefore, the 2nd spatial harmonic is selected for the analysis, and the simulated 2nd harmonic is shown in Fig. 15. Fig. 15 demonstrates that by applying the proposed model, the amplitude of the 2nd harmonic is decreased by 45% from the conventional design.

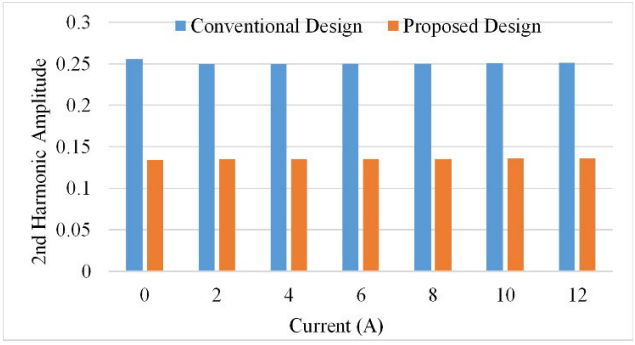

FIGURE 15. 2nd harmonics of airgap flux density of the conventional and proposed design.

The 2nd harmonic amplitude doesn't eliminate in the proposed design; however, it was much smaller than the existing design; thus, the magnet eddy current loss reduced considerably. Only the 2nd harmonic were examined here; nevertheless, these principles can also be used for analysis of other harmonics. The slightly increased behavior is observed in the

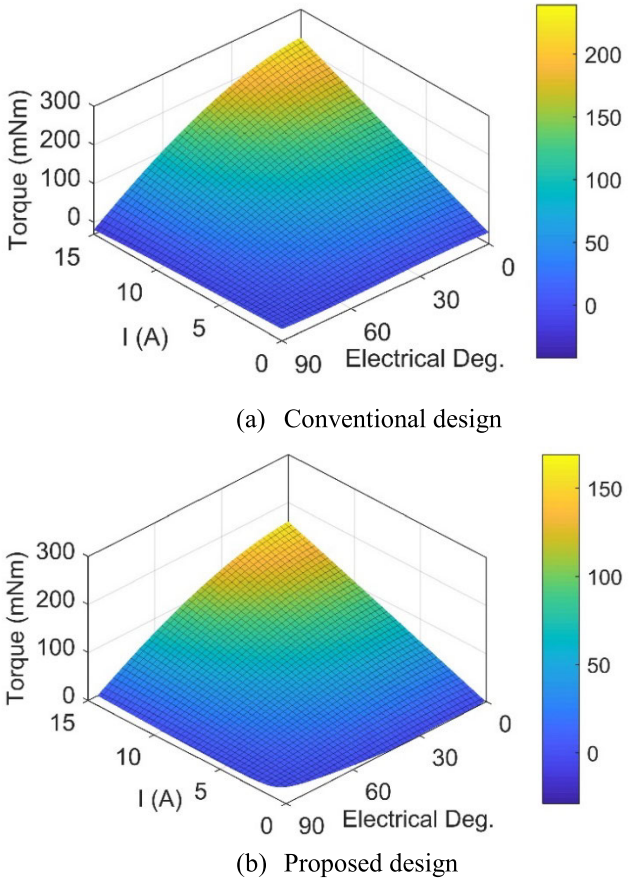

FIGURE 16. Comparison of output torque at various conditions.

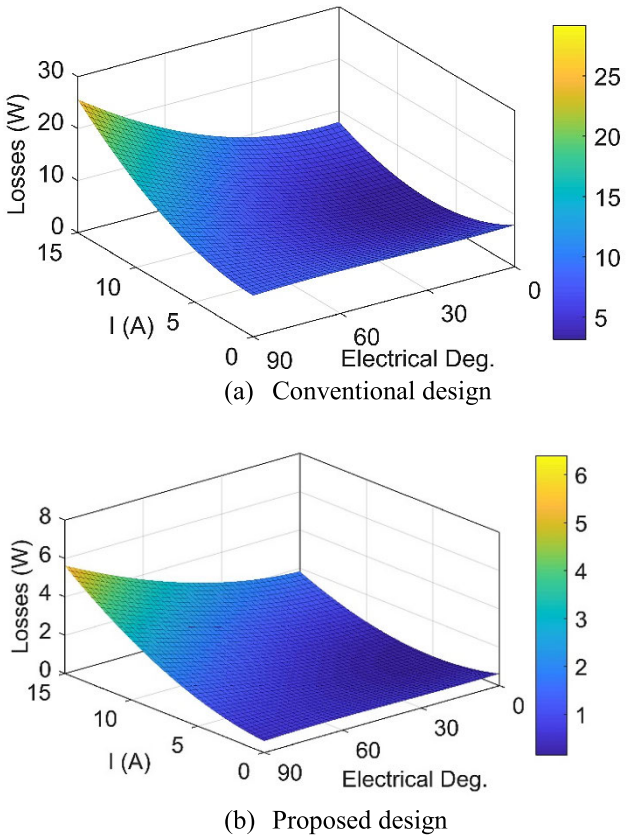

FIGURE 17. Magnet eddy current loss in conventional vs. proposed design.

amplitude of airgap flux density 2nd harmonic corresponding to the input current at different operating conditions.

V. ANALYZING LOSSES AND TORQUE AT VARIOUS OPERATING CONDITIONS

In the previous section, the electromagnetic performance of proposed design was addressed at rated current density. Nevertheless, the rated conditions can be change; consequently, an analysis at various current density is necessary. The output torque and PM eddy current loss of conventional and proposed design is demonstrated in Fig. 16 (a), (b), and Fig. 17 (a), (b) respectively. The figures show that the change in the angle of current slightly influences PM to eddy current loss. Whereas an increase in the magnitude of input current significantly increases the losses in the existing design. In contrast, a slight effect on the magnet eddy current loss occurs corresponding to the proposed design's current amplitude and angle. Consequently, PM eddy current losses in the proposed design are considerably reduced than the existing design at various operating conditions. The eddy current losses are decreased by 78.7%, at a current amplitude of 15 A and 90° angle compared with the existing design. However, the proposed design has less electromagnetic torque throughout the operating range.

In the proposed design, the average torque was lower than that of the existing model; hence, deterministic optimization technique (single variable optimization) was used to optimized the proposed design.

VI. OPTIMIZATION OF THE PROPOSED DESIGN

The initial design is optimized to achieve optimal performance by updating defined parameters of rotor, stator, and sleeve, as illustrated in Fig. 18. The targeted output torque of 148mNm is expected to achieve in the optimized design. A deterministic optimization technique shown in Fig. 19 improves the proposed model's torque by optimizing the stator pole and yoke width. The permanent magnet and airgap volume are kept constant, while the free parameters S1, S2, and S3 are changed.

The optimization procedure reduces the stator pole and yoke width, increasing the stator slots area at fixed armature current density. The increase in stator slot results in changing the number of turns and hence electric loading. The current density and filling factor of 4.47A/mm^2 and 0.5, respectively, were determined from the conventional design. The number of turns for the armature coil is calculated from Eq. (17).

$$N_a = \frac{J_a S_a \alpha}{I_a}, \tag{17}$$

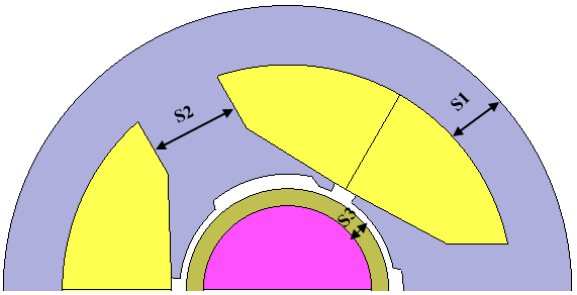

FIGURE 18. Design parameters of optimization.

where J_a, α, S_a, I_a, and N_a are current density, filling factor, area of the slot, input current, and the number of turns, respectively.

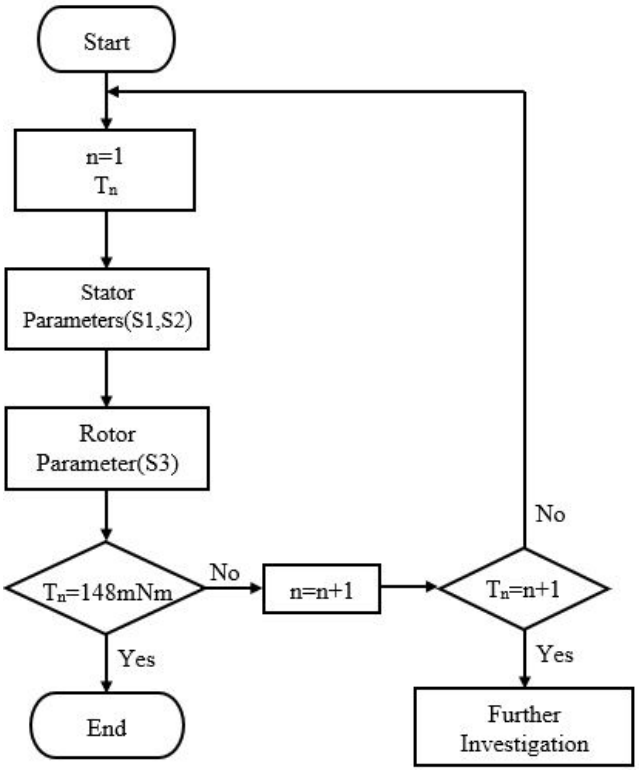

FIGURE 19. Flow chart of the optimization process.

In the optimization process, shown in Fig. 19 the stator parameters are updated initially; the stator yoke size S1 is the first modified parameter due to its dominant effect, where torque is directly proportional to the increase in the internal radius of the stator. Nevertheless, too much decrease in S1 while keeping the stator pole depth constant will reduce back iron length, causing limitation of flux flow resulting in yoke saturation. Therefore, the yoke size S1 was optimized according to the allowable constraints. The stator yoke width S1 is kept constant once the maximum torque is achieved, and S2 and S3 are then optimized. Optimizing the stator pole width S2 and sleeve width S3 can also improve the performance

TABLE 3. Design parameters.

Proposed		Optimized	
Geometry Parameters	Value	Geometry Parameters	Value
Outer diameter of the stator	50 mm	Outer diameter of the stator	50 mm
Height of yoke	5.2 mm	Height of yoke	4 mm
Pole width	8 mm	Pole width	5 mm
Sleeve thickness	1.5 mm	Sleeve thickness	1.3 mm

of the proposed design. However, too narrow stator pole and sleeve width will inhibit optimal flux from flowing and tend to degrade the machine's performance. Hence, parameters S1, S2, S3 are optimized with the constraints that the pole, yoke, and sleeve are not saturated.

The optimization process and modification of design parameters are iterated until the optimum output torque is achieved. It is found that the most dominant parameters that affect the output torque were S1 and S2, while S3 has a slight effect on the electromagnetic torque density. The difference between the parameters of the proposed and optimized design are shown in Table. 3. The optimized design armature slot has a 28.2% higher area than the proposed model to achieve the optimum magnetic flux and maximum output torque performance. The applied armature current is kept constant for the optimized electric loading, while the number of turns is adjusted to get the desired output torque.

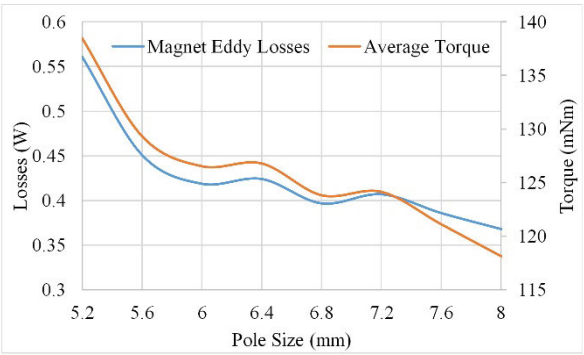

FIGURE 20. Magnet Eddy current losses and output torque vs. pole size.

A. OPTIMAL DESIGN OF POLE

Fig. 20 shows the influence of pole width on the output electromagnetic torque and PM eddy current losses. It is found that the relationship between pole size and output torque is inversely proportional. The figure illustrates that the stator pole has a significant influence on eddy current losses, which increases by 33.9% with a decrease in pole width. Meanwhile, the proposed design electromagnetic torque has not linearly reduced corresponding to the rise in the pole's

TABLE 4. Different parameters comparison.

Parameters	Optimized	Proposed	Conventional
Rated torque	160 mN·m	118.3 mN·m	148.7 mN·m
Cogging torque	8.6 mN·m	7.1 mN·m	27 mN·m
Flux linkages	23.2mWb	18.6 mWb	20.1 mWb
Iron losses	177.86 W	127.7 W	230 W
Magnet eddy current loss	0.51 W	0.25 W	1.89 W

width; however, the impact of pole width is relatively high, which decreases the value of electromagnetic torque from 139.2 mN · m to 119 mN · m.

B. OPTIMIZED DESIGN OF BACK IRON LENGTH

The effect of yoke width on magnet eddy current loss and electromagnetic torque is illustrated in Fig. 21. The yoke width decreases from 5.2mm to 4mm with a gradual decrease of 0.2 mm. Once the maximum torque is attained, the width of the yoke is kept constant, and the size of the pole is modified. Fig. 21 signifies that the influence of yoke width has the same behavior on electromagnetic torque and magnet eddy current loss. The reduction in yoke width from 5.2 mm to 4 mm increases PM eddy current loss by 28%. In contrast, the output electromagnetic torque increases by 20.2%, with the corresponding reduction in yoke width.

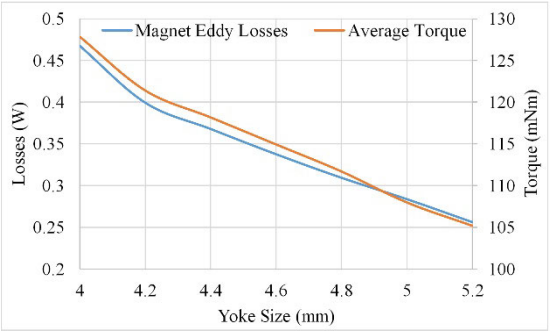

FIGURE 21. Width of yoke vs. output electromagnetic torque and magnet eddy current losses.

Table. 4 shows the peak-to-peak values of optimized design FEA outcomes at no-load and loaded conditions. After applying optimization, the proposed model flux linkage is increased by 13.3% from the conventional model. Compared with the proposed model, the cogging torque of the optimized model rose slightly: however, it is smaller than the conventional design. At the maximum current density of 4.45A/mm^2, the optimized design electromagnetic torque increases by 26% from the proposed design.

VII. CONCLUSION

During the design process of high-speed PM machines, special attention must be paid to design issues. High-speed PM machines can provide excellent performance in terms of controllability, energy efficiency, and torque density. However, at critical speed operations, PMs on the rotor are prone to centrifugal force, which may break their physical integrity. Therefore, the PMs are retained by alloy sleeves or bound with an enclosure on the rotor surface. This paper proposes a novel motor design using titanium enclosure for a solid permanent magnet rotor considering mechanical, electromagnetic, and thermal aspects.

The analysis shows that the proposed model has reduced cogging torque, eddy current loss of PM and iron losses at various operating conditions by 87.6%, 70% and 44.5% respectively. A 2D finite element method (FEM) is used to compute a precise rotor sleeve stress. The proposed model is also optimized for high output torque using deterministic optimization technique. The proposed optimized 3-slot/2-pole design with updated parameters has high output performance in terms of electromagnetic output torque at various input current compared to conventional design. The output average electromagnetic output torque is improved by 26.065% compared to the initial design.

REFERENCES

[1] G. Du, W. Xu, J. Zhu, and N. Huang, "Effects of design parameters on the multiphysics performance of high-speed permanent magnet machines," *IEEE Trans. Ind. Electron.*, vol. 67, no. 5, pp. 3472–3483, May 2020.
[2] A. Tenconi, S. Vaschetto, and A. Vigliani, "Electrical machines for high-speed applications: Design considerations and tradeoffs," *IEEE Trans. Ind. Electron.*, vol. 61, no. 6, pp. 3022–3029, Jun. 2014.
[3] P.-D. Pfister and Y. Perriard, "Very-high-speed slotless permanent-magnet motors: Analytical modeling, optimization, design, and torque measurement methods," *IEEE Trans. Ind. Electron.*, vol. 57, no. 1, pp. 296–303, Jan. 2010.
[4] D.-K. Hong, B.-C. Woo, J.-Y. Lee, and D.-H. Koo, "Ultra high speed motor supported by air foil bearings for air blower cooling fuel cells," *IEEE Trans. Magn.*, vol. 48, no. 2, pp. 871–874, Feb. 2012.
[5] C. Zhang, L. Chen, X. Wang, and R. Tang, "Loss calculation and thermal analysis for high-speed permanent magnet synchronous machines," *IEEE Access*, vol. 8, pp. 92627–92636, 2020.
[6] X. Zhao, B. Kou, L. Zhang, and H. Zhang, "Design and analysis of permanent magnets in a negative-salient permanent magnet synchronous motor," *IEEE Access*, vol. 8, pp. 182249–182259, 2020.

[7] C. Di, I. Petrov, and J. J. Pyrhonen, "Extraction of rotor eddy-current harmonic losses in high-speed solid-rotor induction machines by an improved virtual permanent magnet harmonic machine model," *IEEE Access*, vol. 7, pp. 27746–27755, 2019.
[8] B. Hannon, P. Sergeant, and L. Dupré, "Time- and spatial-harmonic content in synchronous electrical machines," *IEEE Trans. Magn.*, vol. 53, no. 3, pp. 1–11, Mar. 2017.
[9] V. Abramenko, J. Nerg, I. Petrov, and J. Pyrhonen, "Influence of magnetic and nonmagnetic layers in an axially laminated anisotropic rotor of a high-speed synchronous reluctance motor including manufacturing aspects," *IEEE Access*, vol. 8, pp. 117377–117389, 2020.
[10] N. Ahmad, F. Khan, H. A. Khan, S. Khan, F. Khan, M. A. Khan, and I. Ahmad, "Effective computational techniques of reducing cogging torque in permanent magnet flux switching machine," *J. Appl. Emerg. Sci.*, vol. 10, no. 1, p. 19, 2020.
[11] Y. Wang, J. Ma, C. Liu, G. Lei, Y. Guo, and J. Zhu, "Reduction of magnet eddy current loss in PMSM by using partial magnet segment method," *IEEE Trans. Magn.*, vol. 55, no. 7, pp. 1–5, Jul. 2019.
[12] Q. Chen, D. Liang, S. Jia, and X. Wan, "Analysis of multi-phase and multi-layer factional-slot concentrated-winding on PM eddy current loss considering axial segmentation and load operation," *IEEE Trans. Magn.*, vol. 54, no. 11, pp. 1–6, Nov. 2018.
[13] K. Yamazaki, Y. Togashi, T. Ikemi, S. Ohki, and R. Mizokami, "Reduction of inverter carrier harmonic losses in interior permanent magnet synchronous motors by optimizing rotor and stator shapes," *IEEE Trans. Ind. Appl.*, vol. 55, no. 1, pp. 306–315, Jan. 2019.
[14] B. Hannon, P. Sergeant, and L. Dupre, "Evaluation of the rotor eddy-current losses in high-speed PMSMs with a shielding cylinder for different stator sources," *IEEE Trans. Magn.*, vol. 55, no. 3, pp. 1–10, Mar. 2019.
[15] H.-W. Jun, J.-W. Lee, G.-H. Yoon, and J. Lee, "Optimal design of the PMSM retaining plate with 3-D barrier structure and eddy-current loss-reduction effect," *IEEE Trans. Ind. Electron.*, vol. 65, no. 2, pp. 1808–1818, Feb. 2018.
[16] S. Jumayev, M. Merdzan, K. O. Boynov, J. J. Paulides, J. Pyrhonen, and E. Lomonova, "The effect of PWM on rotor eddy-current losses in high-speed permanent magnet machines," in *Proc. IEEE Magn. Conf. (INTERMAG)*, Beijing, China, May 2015, p. 1.
[17] J. Ma and Z. Q. Zhu, "Magnet eddy current loss reduction in permanent magnet machines," *IEEE Trans. Ind. Appl.*, vol. 55, no. 2, pp. 1309–1320, Mar. 2019.
[18] F. Zhang, G. Du, T. Wang, G. Liu, and W. Cao, "Rotor retaining sleeve design for a 1.12-MW high-speed PM machine," *IEEE Trans. Ind. Appl.*, vol. 51, no. 5, pp. 3675–3685, Oct. 2015.
[19] H. A. Khan, F. Khan, N. Ahmad, and J.-S. Ro, "Analysis and design of novel high speed permanent magnet machine considering magnet eddy current loss," *IEEE Access*, vol. 8, pp. 135675–135685, 2020.
[20] Z. Zhu, Y. Huang, J. Dong, F. Peng, and Y. Yao, "Rotor eddy current loss reduction with permeable retaining sleeve for permanent magnet synchronous machine," *IEEE Trans. Energy Convers.*, vol. 35, no. 2, pp. 1088–1097, Jun. 2020.
[21] L. Li, W. Li, D. Li, X. Zhang, and Y. Fan, "Influence of sleeve thickness and various structures on eddy current losses of rotor parts and temperature field in surface mounted permanent-magnet synchronous motor," *IET Electr. Power Appl.*, vol. 12, no. 8, pp. 1183–1191, Sep. 2018.
[22] G. Du, W. Xu, J. Zhu, and N. Huang, "Rotor stress analysis for high-speed permanent magnet machines considering assembly gap and temperature gradient," *IEEE Trans. Energy Convers.*, vol. 34, no. 4, pp. 2276–2285, Dec. 2019.
[23] Y. Wang, Z. Q. Zhu, J. Feng, S. Guo, Y. F. Li, and Y. Wang, "Rotor stress analysis of high-speed permanent magnet machines with segmented magnets retained by carbon-fibre sleeve," *IEEE Trans. Energy Convers.*, early access, Sep. 8, 2020, doi: 10.1109/TEC.2020.3022475.
[24] M. Zheng, W. Huang, and C. Gao, "Rotor stress and dynamics analysis of a high-speed permanent magnet machine for a micro gas turbine considering multiphysics factors," *IEEE Access*, vol. 8, pp. 152523–152531, 2020.
[25] G. Burnand, D. M. Araujo, and Y. Perriard, "Very-high-speed permanent magnet motors: Mechanical rotor stresses analytical model," in *Proc. IEEE Int. Electric Mach. Drives Conf. (IEMDC)*, Miami, FL, USA, May 2017, pp. 1–7.
[26] F. Chai, Y. Li, P. Liang, and Y. Pei, "Calculation of the maximum mechanical stress on the rotor of interior permanent-magnet synchronous motors," *IEEE Trans. Ind. Electron.*, vol. 63, no. 6, pp. 3420–3432, Jun. 2016.
[27] S. Wu, X. Huang, L. He, S. Cui, and W. Zhao, "Mechanical strength analysis of pulsed alternator air-core rotor," *IEEE Trans. Plasma Sci.*, vol. 47, no. 5, pp. 2387–2392, May 2019.
[28] I. Kleilat, K. El Kadri Benkara, G. Friedrich, S. Vivier, N. Moubayed, and R. Dib, "Comparison of two analytical methods for calculating the maximum mechanical stress in the rotor of high speed assisted synchronous reluctance machines," *IEEE Trans. Ind. Appl.*, early access, Nov. 26, 2020, doi: 10.1109/TIA.2020.3040946.
[29] G. Chu, R. Dutta, H. Lovatt, B. Sarlioglu, and M. F. Rahman, "Analytical calculation of maximum mechanical stress on the rotor of the interior permanent-magnet synchronous machine," in *Proc. IEEE Energy Convers. Congr. Expo. (ECCE)*, Portland, OR, USA, Sep. 2018, pp. 255–261.
[30] K.-H. Shin, T.-K. Bang, H.-W. Cho, and J.-Y. Choi, "Design and analysis of high-speed permanent magnet synchronous generator with rotor structure considering electromechanical characteristics," *IEEE Trans. Appl. Supercond.*, vol. 30, no. 4, pp. 1–5, Jun. 2020.
[31] A. Binder, T. Schneider, and M. Klohr, "Fixation of buried and surface-mounted magnets in high-speed permanent-magnet synchronous machines," *IEEE Trans. Ind. Appl.*, vol. 42, no. 4, pp. 1031–1037, Jul. 2006.
[32] L. Chen and C. Zhu, "Rotor strength analysis for high speed permanent magnet machines," in *Proc. 17th Int. Conf. Electr. Mach. Syst. (ICEMS)*, Hangzhou, China, Oct. 2014, pp. 65–69.
[33] L. Ur Rahman, F. Khan, M. A. Khan, N. Ahmad, H. A. Khan, M. Shahzad, S. Ali, and H. Ali, "Modular rotor single phase field excited flux switching machine with non-overlapped windings," *Energies*, vol. 12, no. 8, p. 1576, Apr. 2019.

HAMID ALI KHAN was born in Swat, Khyber Pakhtunkhwa, Pakistan. He received the B.S. and M.S. degree in electrical engineering from COMSATS University Islamabad, Attock and Abbottabad campus, Pakistan, in 2017 and 2020, respectively. From 2017 to 2020, he was a Research Assistant with the Electric Machine Design Research Laboratory, Electrical and Computer Engineering Department, COMSATS University Islamabad, Abbottabad Campus, focuses on designing and analysis of high speed electrical machines. From 2019 to 2020, he was a Visiting Research Exchange Scholar with the College of Mechatronics and Control Engineering, Shenzhen University, Shenzhen, China. His current research interests include design, analysis, optimization of high speed electrical machines, and permanent magnet synchronous machines.

FAISAL KHAN (Member, IEEE) was born in Utmanzai, Charsadda, Khyber Pakhtunkhwa, Pakistan, in 1986. He received the B.S. degree in electronics engineering and the M.S. degree in electrical engineering from the COMSATS Institute of Information Technology Islamabad, Abbottabad Campus, Pakistan, in 2009 and 2012, respectively, and the Ph.D. degree in electrical engineering from Universiti Tun Hussein Onn Malaysia, Malaysia, in 2017.

From 2010 to 2012, he was a Lecturer with the University of Engineering and Technology, Peshawar, Abbottabad Campus. Since 2017, he has been an Assistant Professor with the Electrical and Computer Engineering Department, COMSATS University Islamabad, Abbottabad Campus, where he is currently the Head of Electric Machine Design Research Laboratory. He is the author of more than 80 publications. His research interests include design of flux-switching, synchronous, induction, linear, and dc machines. He received multiple research awards.

SURAT KHAN received the bachelor's degree in electrical engineering from the Balochistan University of Engineering and Technology Khuzdar, Pakistan, in 1996, the M.S. degree in telecommunication engineering management from the University of Engineering and Technology, Peshawar, Pakistan, in 2007, and the Ph.D. degree in management science and engineering from the Beijing University of Posts and Telecommunications (BUPT), Beijing, China.

From 1997 to 2000, he was an Electrical Engineer with SIEMENS Pakistan. From 2000 to 2012, he worked with Pakistan Telecommunication Company Ltd. Since 2013, he has been an Assistant Professor with the Balochistan University of Information Technology, Engineering and Management Sciences (BUITEMS), Quetta, Pakistan. He is currently the Chairperson of Electrical Engineering with the Faculty of Information and Communication Technology, BUITEMS. His research interests include analysis and design of electrical machines, power electronic equipment, and drive controls.

NASEER AHMAD was born in Lakki Marwat, Khyber Pakhtunkhwa, Pakistan, in 1992. He received the bachelor's degree in electrical power engineering from the University of Engineering and Technology, Peshawar, in 2015, and the M.S. degree in electrical engineering from COMSATS University Islamabad, Abbottabad campus, Pakistan, in 2018.

Since October 2019, he has been a Lecturer with the Electrical Engineering Department, Balochistan University of Information Technology, Engineering and Management Sciences (BUITEMS), Quetta, Pakistan. His research interests include design and optimization of outer rotor flux switching machine, flux reversal machines, and synchronous machines.

JAHANGEER BADAR SOOMRO received the B.E. degree in electornics engineering and the M.E. degree in electrical power system from Mehran University of Engineering & Technology, Jamshoro. He is currently pursuing the Ph.D. degree in electrical engineering from Sukkur IBA University, Pakistan. He is also an Assistant Professor and a Principle Investigator of Power Hardware in Loop Laboratory, Electrical Department, Sukkur IBA University. His research interests include power quality analysis of power converters, PWM techniques to control power converters, PWM inverters, and real time simulation of power converters.

IRFAN SAMI received the B.Sc. degree in electrical engineering from the University of Engineering and Technology, Peshawar, Bannu Campus, Pakistan, in 2016, and the M.Sc. degree in electrical engineering from COMSATS University Islamabad, Abbottabad Campus, Pakistan, in 2019. He is currently pursuing the Ph.D. degree in electrical engineering with the Chung-Ang University, Seoul, South Korea. His research interests include electric drives, renewable energies, and electrical machine design.